applied sciences

MDPI

Article

General Analytical Method to Predict the Spatial–Temporal Distribution of Extreme Pressure in High-Speed Railway Tunnels in the Post-Train Stage

Wenchao Lv, Angui Li *, Haihang Cui and Li Chen

School of Building Services Science and Engineering, Xi'an University of Architecture and Technology, Xi'an 710055, China

* Correspondence: liag@xauat.edu.cn; Tel.: +86-29-82205958

Abstract: Long-duration aerodynamic pressure fluctuation in high-speed railway tunnels in the post-train stage causes fatigue damage to tunnel structures and facilities. It increases the risk of accidents and requires in-depth research. This complex phenomenon is caused by the superposition of multiple pressure waves generated successively when a train enters/leaves a tunnel. In this study, the spatial–temporal distribution of the pressure state (SDPS) model was developed, and general equations describing the transient pressure state distribution were given. Furthermore, a prediction method for extreme pressures in tunnels and a fast calculation program were proposed based on the SDPS model. The proposed model was verified using field measurements. Using the SDPS model, the worst conditions of pressure fluctuations in tunnels were analyzed. The results show that most of the maximum positive and negative pressures are symmetrical around the midpoint of the tunnel axis and appear alternately around it. When the train/wave velocity ratio $M \leq 0.8$ and the train/tunnel length ratio $\varepsilon \leq 0.8$, the dimensionless position of the maximum peak-to-peak pressure region was concentrated in the region of [0.33,0.67] in the tunnel, indicating the location of potential fatigue damage. The proposed model is helpful in building safe and sustainable transportation systems.

Keywords: high-speed railway tunnel; pressure wave; maximum pressure; maximum peak-to-peak pressure; fatigue failure; safe transportation systems

Citation: Lv, W.; Li, A.; Cui, H.; Chen, L. General Analytical Method to Predict the Spatial–Temporal Distribution of Extreme Pressure in High-Speed Railway Tunnels in the Post-Train Stage. *Appl. Sci.* **2023**, *13*, 1350. https://doi.org/10.3390/app13031350

Academic Editor: Hassan Hemida

Received: 30 December 2022
Revised: 13 January 2023
Accepted: 16 January 2023
Published: 19 January 2023

1. Introduction

As a high-speed train travels through a tunnel, pressure waves are generated due to the restricted airspace within the tunnel and the compressibility of the air. When the train nose and tail enter or leave a tunnel, the local flow and cross-section dramatically change, successively causing four pressure wave systems (PWSs) at the portals of the tunnel. With the reciprocating propagation, reflection, and superposition of pressure waves, long-duration and large-amplitude pressure fluctuations are generated inside tunnels and act on the tunnel and train surface, producing alternating loads. It affects the crack initiation and propagation in the structure [1]; causes high-cycle fatigue damage to train structures [2,3], tunnel structures [4–6], and pressure-bearing tunnel facilities (including fire doors, control boxes, signal lights, etc.) [3,7,8]; and leads to vibration discomfort for passengers [9], threatening the safety of transportation systems [10,11]. For example, in 1999, influenced by long-term aerodynamic loads, a block of lining detached from the Rebunhama high-speed railway tunnel in Japan, which caused train derailment and the cancellation of 51 subsequent trains [1,12]. More importantly, compared with the train passing stage, pressure fluctuation in the post-train stage (after a train exits from a tunnel) has a longer duration and slower attenuation as there is no interaction between the wave and the train [13], but the pressure amplitude is similar or even higher. For example, after a train left a 2812-m-long tunnel at a speed of 300 km/h, the maximum pressure fluctuation in the tunnel was up to 5 kPa. Additionally, it lasted over 60 s before decaying to 50% of the amplitude, which is almost twice the train passing time of 36 s [8,14]. Similar results were found in field measurements [15], scaled-model experiments [13], and numerical simulations [4,16]. Additionally, Du et al. [1] found that damage accumulation in the post-train stage is approximately equal to that during the train-passing stage, indicating that the aerodynamic effects in the post-train stage cannot be ignored. Currently, several researchers have discussed the spatial distribution of extreme pressure in tunnels during train passage [17–19]. However, research concerning pressure changes in the post-train stage is still limited, and the spatial–temporal distribution law of extreme pressure is not clear. Therefore, it is necessary to investigate the spatial–temporal distribution of the typical pressure (extreme pressure and maximum peak-to-peak pressure) after train passage, revealing the locations of potential accidents caused by fatigue failure in tunnels.

The research methods for investigating pressure waves in tunnels include field measurements [8,14,18,20], moving model tests [13,21,22], numerical simulations [4,23], and theoretical analysis [24–26]. However, field measurements and moving model tests are usually expensive and limited by the existing test conditions, and numerical simulations with three-dimensional models consume a lot of computing resources and time [23,27–29]. Additionally, the above methods are all difficult when trying to meet the needs of rapid decision-making with the lowest resource consumption, especially in engineering design.

Theoretical analysis is useful for predicting pressure waves in tunnels. As the length of a tunnel is obviously longer than the tunnel's hydraulic diameter, and the propagation time of the pressure in the cross-section is much less than that along the tunnel, it exhibits typical one-dimensional geometric and kinematic characteristics. In the post-train stage especially, only the pressure wave continuously propagates, reflects, and superposes in the tunnel. Therefore, a one-dimensional theoretical model has been proposed to obtain the pressure characteristics in the tunnel. Based on this, semi-theoretical and semi-empirical equations are proposed in combination with on-site tests or moving model measurements to describe the initial waveform of the entry compression wave with variations in time or space, written as $p(t)$ and $p(x)$, respectively [30,31]. The one-dimensional model has been validated using field measurements [13,14] and numerical simulations [32], but it still has some deficiencies. First, due to the evolution and superposition of the pressure waves, the pressure varies with time and space simultaneously, which is more accurately described as $p(x, t)$. Second, the equations in the one-dimensional model need to calculate the pressure of any point at any time from the flow and pressure states of the adjacent positions at the previous moment using 1D finite volume methods [33,34] or 1D finite difference [15,35], which requires lots of iterative calculations. At the same time, it is notable that the pressure state of any point in the tunnel is the sum of the state influenced by each pressure wave individually at a given time, which is independent of the state of adjacent positions at the previous moment. Thus, based on the principle of superposition, it is possible to develop more accurate equations to describe the pressure state changes over time and space $p_s(x, t)$ without iterative calculations.

Based on the superposition of four PWSs in a tunnel, a one-dimensional model, referred to as the spatial–temporal distribution of the pressure state (SDPS) model, is proposed, and equations are first proposed to describe the transient pressure state at any point in a tunnel $p_s(x, t)$. To identify the extreme pressure in the post-train stage, a spatial–temporal prediction method and a calculation program are proposed. Additionally, two dimensionless quantities, namely the train/wave velocity ratio M and the train/tunnel length ratio ε, are proposed to describe the operating conditions based on dimensionless analysis. Then, the dimensionless spatial–temporal distribution characteristics of the extreme parameters (including the maximum positive pressure (MPP), the maximum negative pressure (MNP), and the maximum peak-to-peak pressure region (MPPR)) under different cases were analyzed, indicating the location of potential fatigue failure in tunnels. This study is helpful when attempting to understand the spatial–temporal distribution of pressure in a tunnel and to identify regions that have a high risk of fatigue failure at an early stage.

2. Spatial–Temporal Evolution of Pressure Waves in a Tunnel

The generation, propagation, reflection, and superposition mechanism of complex pressure waves in tunnels are shown in Figure 1. It shows the pressure time histories at 140 m from the entrance and the associated wave diagram when a 201.4-m-long train passes through a 1005-m-long tunnel at a speed of 300 km/h (the local velocity of sound c is 336 m/s) [36]. The solid and dashed lines represent the compression and expansion waves, respectively, which are generated when the train enters/leaves the tunnel. The train nose entry/exit generates a compression wave propagating throughout the tunnel, resulting in a pressure increase (corresponding to the labels 1, 6–7, 10–12, 17–20, and 25–28 in Figure 1). At the same time, the train tail entry/exit generates an expansion wave causing a pressure drop (corresponding to the labels 3, 5, 8–9,13–16, 21–24, and 29 in Figure 1). Both the compression wave and the expansion wave propagate backward and forward in the tunnel at the local velocity of sound *c*. Each time the pressure wave reaches the tunnel portals, it reflects backward, and the reflected wave is out-of-phase with the incident one [18]. As pressure waves can be described by linear equations, the principle of superposition is applicable [37,38]. That is, the pressure change caused by two or more pressure waves is the sum of the change caused by each wave individually.

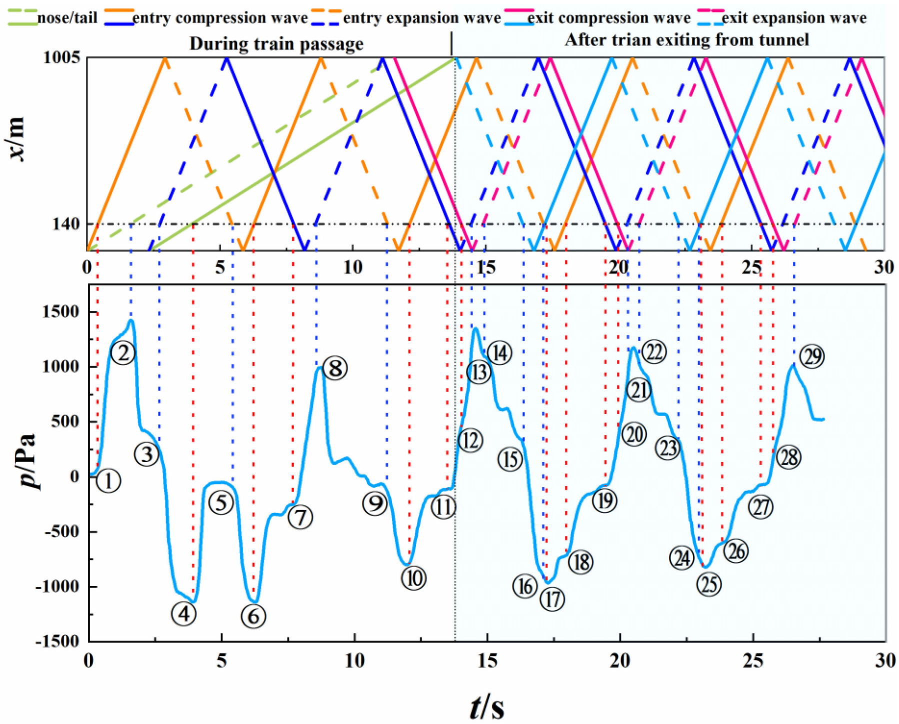

Figure 1. Pressure time histories at 140 m and associated wave diagram for a 201.4-m-long train passing through a 1005-m-long tunnel at 300 km/h (adapted from Liu et al. [36]).

In this paper, the complex pressure waves are divided into four categories. As shown in Figure 2, according to the time sequence, the first is nose-entry-induced PWS, which includes the train nose-entry-induced compression wave and its reflected waves. The second one is the tail entry-induced PWS, including the tail-entry-induced expansion wave and its reflected waves. The third is the nose-exit-induced PWS, which contains the nose-exit-induced compression wave and its reflected waves. The last is the tail-exit-induced PWS, containing the tail-exit-induced expansion wave and its reflected waves [39,40].

In addition, the passage of the train nose and tail, represented by the green dashed lines and solid lines in Figure 1, also causes a pressure decrease and increase, respectively, due to the induced pressure pulse (PP) [41,42]. The difference between PWS and PP is that PWS propagates to and fro with the velocity of sound *c* while PP does not reflect and moves with the train speed of v_{tr}. It is reported that PPs also have effects on the location of extreme pressure during train passage [18,19]. As shown in Figure 2b, pressure fluctuates in two stages, namely the passing stage and the post-train stage. The pressure fluctuation during train passage is caused by the superposition of two entry-induced PWSs and two PPs induced by the end of the train while the significant pressure fluctuations in the post-train stage consider the superposition of four PWSs (two more exit-induced PWSs) and two PPs. Different superimposed times and locations of the PWSs lead to different spatial distributions of extreme pressure in the tunnel [43].

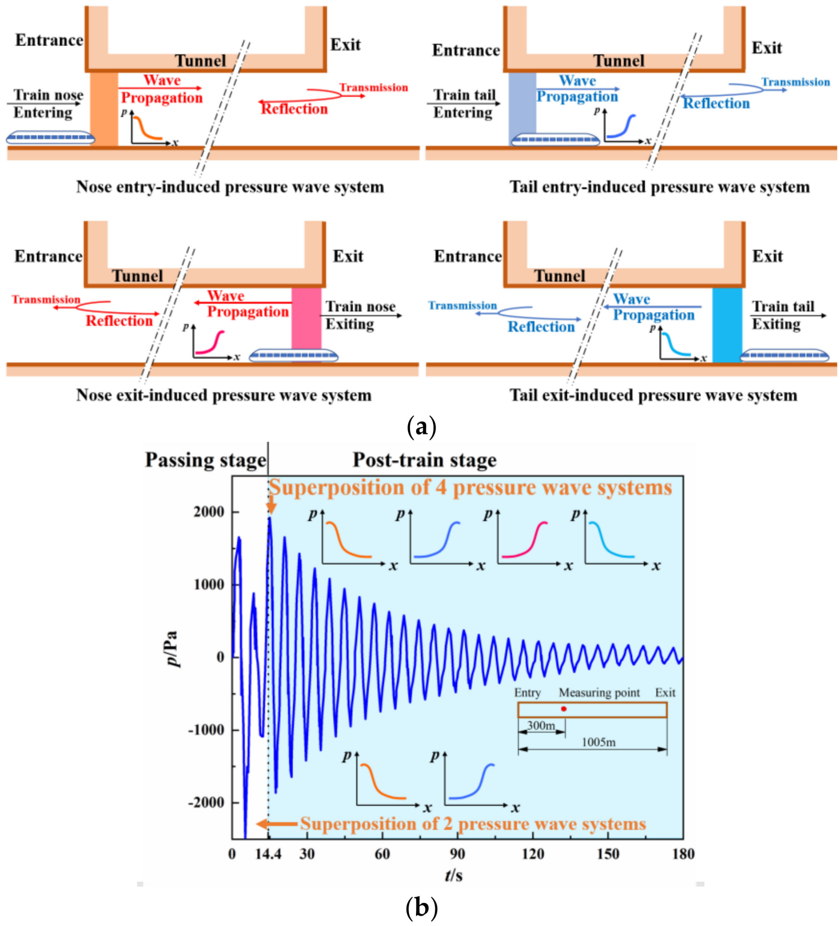

Figure 2. Schematic of pressure fluctuation in two stages: (**a**) Four pressure wave systems induced by a high-speed train entering/exiting from a tunnel; (**b**) Pressure fluctuation of the passing stage and post-train stage. (adapted from Liu et al. [36]).

3. Analytical Method for Spatial–Temporal Prediction of the Extreme Pressure

To investigate the wave effects in tunnels in the post-train stage, an analytical approach is proposed based on a one-dimensional unsteady compressible flow model.

3.1. Assumptions

1. The tunnel is simplified as a long, even, and straight tunnel without shafts, and its cross-sectional area is constant [44];
2. Since the propagation time of the pressure wave in the cross-section is far less than that along the tunnel, the pressure fluctuation in the tunnel cross-section is ignored;
3. The pressure wave is generated at the moment when the train enters or leaves the tunnel, and the wave celerity is approximately the velocity of sound and remains constant during propagation [42];
4. The much weaker wavelet, which is generated by the interaction between pressure and the train/tunnel system during train passage, is neglected when analyzing the location of the extreme pressure in the post-train stage.

3.2. Spatial–Temporal Distribution of Pressure State Model

3.2.1. Distribution of Pressure State Influenced by Press Wave Systems

Take the nose-entry-induced PWS as an example; as shown in Figure 3, with the tunnel entrance as the origin, the coordinate system was established along the tunnel as the x-axis. x = 0 and $x = L_{tu}$ correspond to the tunnel entry and exit, respectively (L_{tu} is the tunnel length). The initial time t = 0 was recorded as the arrival of the train nose at the tunnel entrance, x_w is the position where the pressure wave reaches the tunnel, and p_s represents the pressure state, which is recorded as 1 for a pressure rise and −1 for a pressure drop. For example, when a compression/expansion wave sweeps a point, its pressure state would be +1/−1, accordingly, and remains stable until the next disturbance (PWS or PP) reaches; n_w is the reflected times of the wave at the tunnel port after its generation.

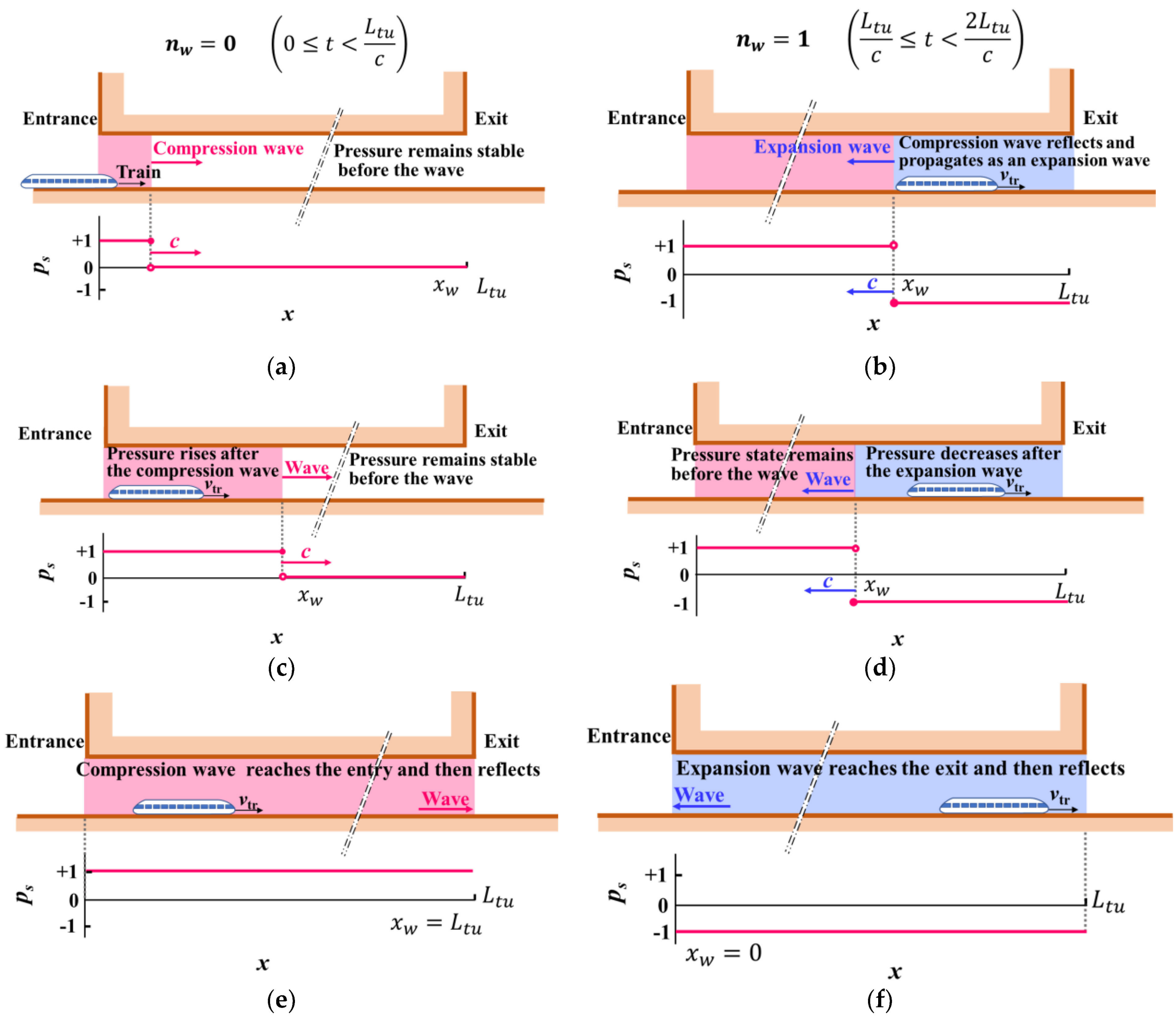

Figure 3. Schematic of pressure wave propagation and the associated distribution of pressure state: (**a**,**c**,**e**) n_w = 0; (**b**,**d**,**f**) n_w = 1. (p_s: pressure state; n_w: the reflected times of the wave at the tunnel port; x_w: the location of pressure wave; L_{tu}: tunnel length; v_{tr}: train speed; c: the velocity of sound).

As shown in Figure 3a,c,e, when the train nose enters the tunnel (t = 0), the nose-entry-induced compression wave generates and moves from the tunnel entry (x_w = 0) to the tunnel exit ($x_w = L_{tu}$), and the corresponding n_w is 0. As shown in Figure 3c, after being swept by the compression wave, the pressure rises, p_s = 1; the pressure state remains unchanged before the wave, p_s = 0.

When the compression wave reaches the tunnel exit ($t = L_{tu}/c$), it reflects and then propagates as an expansion wave, and n_w becomes 1, as shown in Figure 3b,d,f. After being swept by the expansion wave, the pressure decreases, and $p_s = -1$. Before the wave, the pressure state remains and is considered to be influenced by the previous compression wave, and $p_s = 1$, as shown in Figure 3d.

The expansion wave propagates to the tunnel entry at the velocity of sound c; it reaches the entry ($t = 2L_{tu}/c$) and reflects as a compression wave; n_w becomes 2. As shown in Figure 4c, the pressure rises after the compression wave, where $p_s = 1$; before the wave, the pressure state remains and is considered to be influenced by the previous expansion wave, where $p_s = -1$.

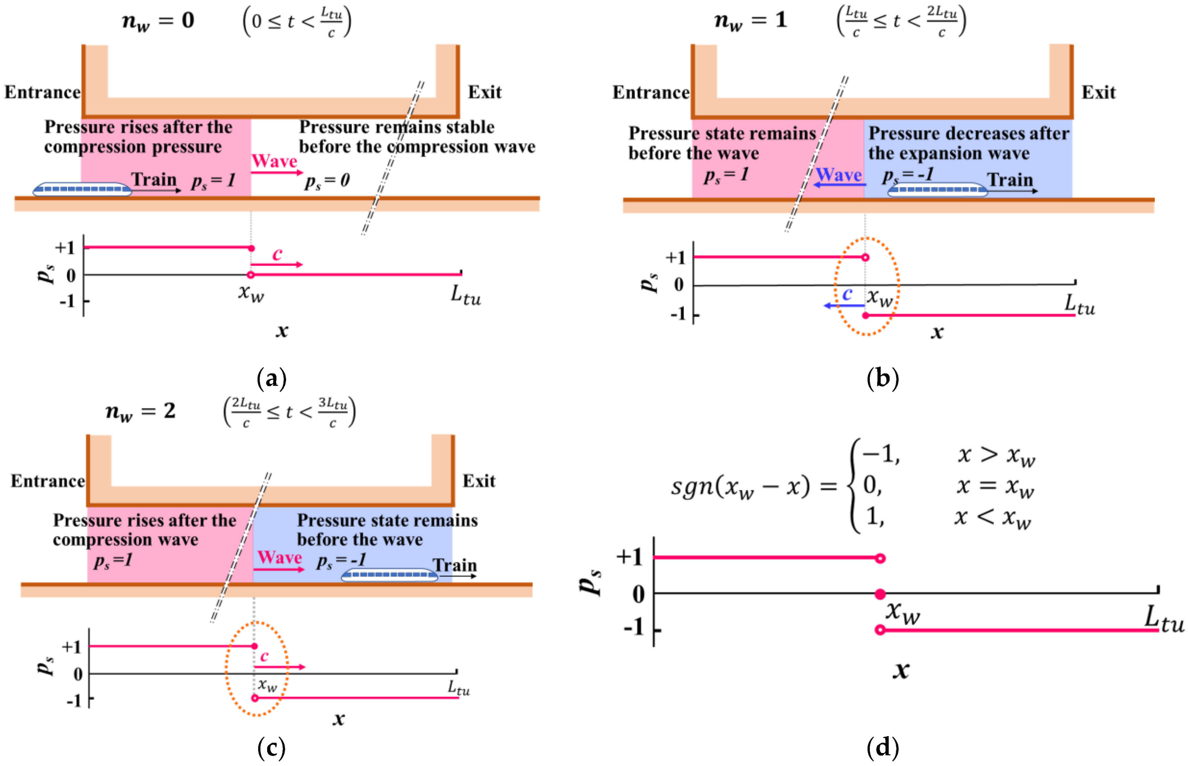

Figure 4. Schematic of pressure state distribution under different n_w: (**a**) $n_w = 0$, (**b**) $n_w = 1$, (**c**) $n_w = 2$, (**d**) Schematic of sign function (n_w: the reflected times of the wave at the tunnel port; p_s: pressure state; x_w: the location of pressure wave; L_{tu}: tunnel length; c: the velocity of sound).

Based on the propagation and reflection characteristics of the PWS, the propagation cycle of PWS is $2L_{tu}/c$. Due to the periodicity of PWS, the pressure state fluctuation in the tunnel is classified into three categories: $n_w = 0$, n_w is odd, and n_w is even. Figure 4 shows the spatial distribution of pressure state $p_s(x)$ in the tunnel when $n_w = 0$, 1, and 2.

As shown in Figure 4, the spatial distribution of the pressure state in the tunnel $p_s(x)$ should be described using a piecewise function. It is notable that, as shown in Figure 4c,d, $p_s(x)$ can be regarded as the sign function $f(x) = sgn(x)$ with different propagation directions. $f(x) = sgn(x)$ returns 1 for a positive number, 0 for the number zero, and -1 for a negative number.

$$sgn(x) = \begin{cases} 1, & x > 0 \\ 0, & x = 0 \\ -1, & x < 0 \end{cases} \tag{1}$$

As shown in Figure 4c, when $n_w = 2$ (represents the cases when n_w is even), $p_s(x)$ can approximately be described by $f(x) = sgn(x_w - x)$, but modifications are needed in the case of $x = x_w$.

The first correction term is based on $f(x) = \delta(x-a)$, as it returns 1 when $x = a$; otherwise, it returns 0. When $a = 0$ especially, $f(x) = \delta(x)$ returns 1 when $x = 0$; otherwise, it returns 0.

$$\delta(x-a) = \begin{cases} 1, & x = a \\ 0, & x \neq a \end{cases} \tag{2}$$

In this situation, the correction term is $f(x) = \delta(x - x_w)$ in the cases when n_w is even, which only returns 1 when $x = x_w$.

It is notable that the difference between Figure 4b,c is $p_s(x_w)$. In Figure 4c, $p_s(x_w) = 1$, represents point x_w being swept by a compression wave and encountering a pressure rise. While in Figure 4b, $n_w = 1$ (represents the cases when n_w is odd), $p_s(x_w) = -1$. It illustrates that point x_w is being swept by an expansion wave and encounters a pressure drop. Then, the corresponding correction term is $f(x) = -\delta(x - x_w)$ for the cases where n_w is odd, which returns -1 when $x = x_w$.

The difference between Figure 4a,c is $p_s(x)$ when $x > x_w$. Then, the second correction term is based on $f(x) = H(x)$, which returns 1 for $x > 0$ and 0 for $x < 0$.

$$H(x) = \begin{cases} 1, & x > 0 \\ 0, & x < 0 \end{cases} \tag{3}$$

In this situation, the correction term is $f(x) = H(x - x_w)$, which returns 1 when $x > x_w$.

In brief, the spatial distribution of the pressure state along the tunnel $p_s(x)$ is as follows:

$$p_s(x) = sgn(x_w - x) + (-1)^{n_w}\delta(x - x_w) + \delta(n_w)H(x - x_w) \tag{4}$$

where $f(x) = sgn(x_w - x)$ is the main body of the function, and the other two terms are the correction terms. $f(x) = (-1)^{n_w}\delta(x - x_w)$ modifies the value of $p_s(x_w)$ so that when $x = x_w$, it returns -1 when n_w is odd and returns 1 when n_w is even. $f(x) = \delta(n_w)H(x - x_w)$ only modifies the case with, and returns 1 for $x > x_w$, which is consistent with the actual situation.

Additionally, n_w and x_w vary with time t and need to be described using a piecewise function. For the nose-entry-induced PWS, $n_w(t)$ is as follows:

$$n_w(t) = \begin{cases} 0, & 0 \leq t < \frac{L_{tu}}{c} \\ 1, & \frac{L_{tu}}{c} \leq t < \frac{2L_{tu}}{c} \\ 2, & \frac{2L_{tu}}{c} \leq t < \frac{3L_{tu}}{c} \\ \ldots & \ldots \end{cases} \tag{5}$$

Thus, one of the piecewise functions, the floor function $f(x) = [x]$, is introduced. It gives the largest integer less than or equal to x. Then, $n_w(t)$ is given by the following:

$$n_w(t) = \left[\frac{ct}{L_{tu}}\right] \tag{6}$$

For example, when $\frac{L_{tu}}{c} \leq t < \frac{2L_{tu}}{c}$, then $1 \leq \frac{ct}{L_{tu}} < 2$, the corresponding n_w is 1.

For the nose-entry-induced PWS, the position of the pressure wave in the tunnel $x_w\ (t)$ is given by the following:

$$x_w(t) = \begin{cases} ct, & n_w(t) = 0 \\ 2L_{tu} - ct, & n_w(t) = 1 \\ ct - 2L_{tu}, & n_w(t) = 2 \\ 4L_{tu} - ct, & n_w(t) = 3 \\ \ldots & \ldots \end{cases} \tag{7}$$

With the help of the floor function, it is rewritten as follows:

$$x_w(t) = (-1)^{n_w(t)}\left(ct - 2\left[\frac{n_w(t)+1}{2}\right]L_{tu}\right) \tag{8}$$

Substitute $n_w = 0, 1, 2, 3, \ldots$ into Equation (8), then Equation (7) is obtained.

This is the calculation of the nose-entry-induced PWS; those for other PWSs are deduced in the same way.

3.2.2. Distribution of Pressure State Influenced by Pressure Pulses

As shown in Figure 5, x_p represents the position where the PP reaches the tunnel at time t. The train nose and its induced PP move from $t = 0$ to $t = L_{tu}/v_{tr}$ (the moment when train nose reaches the exit). The train-tail-induced PP moves from $t = L_{tr}/v_{tr}$ (when the tail enters the tunnel, where L_{tr} is train length) to $t = (L_{tu} + L_{tr})/v_{tr}$ (when the tail reaches the exit). After the passage of the train nose, the pressure decreases due to the induced PP, $p_s = -1$. After the passage of the train tail, the pressure increases, and the corresponding p_s is 1. Subscripts 1 and 2 correspond to the PP caused by the train nose and tail, respectively.

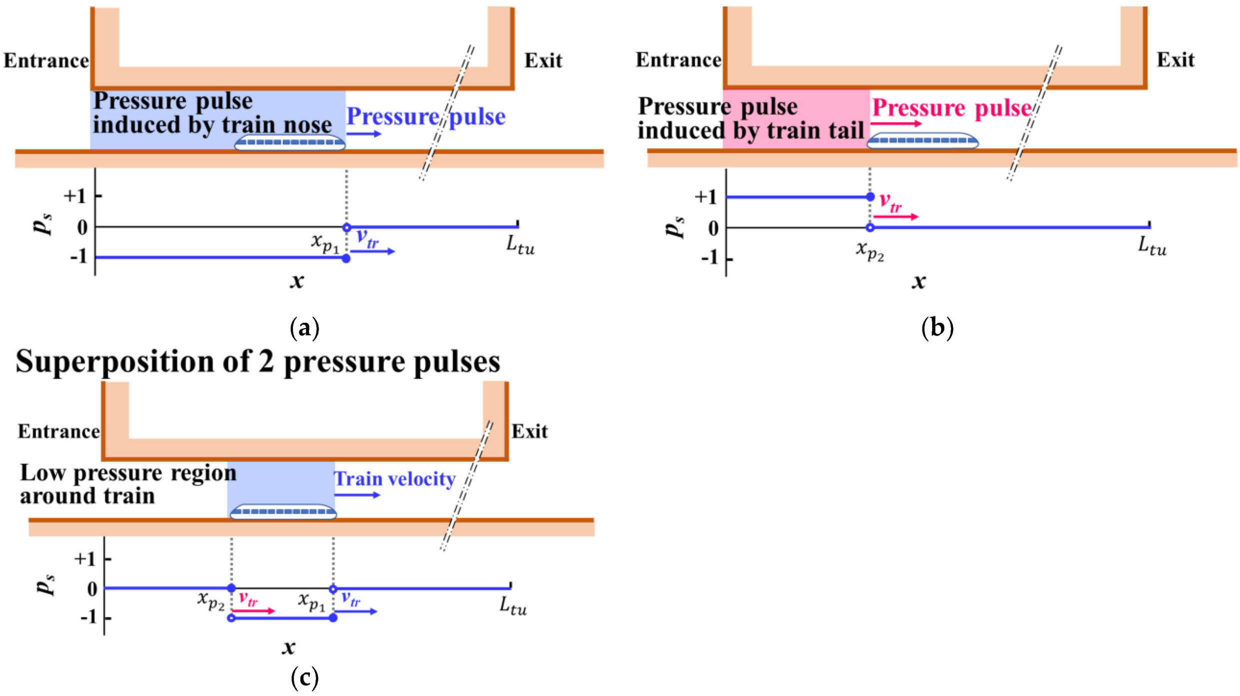

Figure 5. Schematic of p_s distribution caused by pressure pulses: (**a**) p_s distribution influenced by nose-induced pressure pulses, (**b**) p_s distribution influenced by tail-induced pressure pulses, (**c**) p_s distribution influenced by 2 pressure pulses (n_w: the reflected times of the wave at the tunnel port; p_s: pressure state; x_{p1}: the location of pressure pulse induced by train nose; x_{p2}: the location of pressure pulse induced by train tail; L_{tu}: tunnel length; v_{tr}: train speed).

The distribution of the pressure state influenced by PP should also be described using a piecewise function. Then, $f(x) = H(x_p - x)$ is used, and $f(x) = \delta(x - x_p)$ supplements the condition when $x = x_p$. For example, the distribution influenced by nose-induced PP is as follows:

$$\begin{cases} p_{s_{p_1}}(x,t) = -H(x_{p_1}(t) - x) - \delta(x - x_{p_1}(t)) \\ x_{p_1}(t) = v_{tr}t \qquad \left(0 \le t \le \frac{L_{tu}}{v_{tr}}\right) \end{cases} \tag{9}$$

where $x_{p_1}(t)$ shows the path of the nose-induced PP. $p_{s_{p_1}}(x,t)$ returns -1 when $x \le x_{p_1}$, indicating a pressure drop after the passage of the train nose.

Figure 5c shows that the superposition of the two PPs is a relatively low-pressure region around the train and moving with the train speed; it is consistent with the field tests [14] and numerical simulations [45]. Figure 5 shows that for any point in the tunnel, its pressure decreases after the nose passage and increases after the tail passage, which is consistent with the tests [46] and simulations [47].

3.2.3. General Equations of Pressure State Distribution in the Tunnel

Equations (9)–(14) describe the situation where, at time t, the PWS or PP reaches $x_{w\mathrm{i}}$ or $x_{p\mathrm{i}}$ m away from the tunnel entrance. $p_{s_{w_i}}(x,t)$ or $p_{s_{p_i}}(x,t)$ show the spatial–temporal distribution of the pressure state influenced by PWS or PP. The subscript of i = 1, 2, 3, ... is used to distinguish different PWSs and PPs.

Specifically, in Equations (10)–(13), n_w calculates the reflected times of the wave as the pressure wave state (propagates as a compression wave or an expansion wave) and propagation direction changes with different n_w. $x_{w_i}(t)$ describes the propagation path of PWS, and $(-1)^{n_{w_1}(t)}$ describes the wave propagation direction varied with n_w. As mentioned in Section 3.2.1, the first term in the equation of $p_{s_{w_i}}(x,t)$ describes the pressure state distribution approximately; the second term modifies the case when $x = x_w$; and the third term modifies the initial pressure state distribution when $n_w = 0$. Additionally, t_0 and t_1 are used to describe the PWSs, which are generated at different times. For the nose-entry-induced PWS, it generates when the train nose enters the tunnel (t = 0), the tail-entry-induced PWS generates when the train tail enters the tunnel ($t = L_{tr}/v_{tr}$), the nose-exit-induced one generates when the nose leaves the tunnel ($t = L_{tu}/v_{tr}$), and the tail-exit-induced one appears when the tail exits from the tunnel ($t = (L_{tu} + L_{tr})/v_{tr}$).

(1) Nose-entry-induced PWS

$$\begin{cases} p_{s_{w_1}}(x,t) = sgn(x_{w_1}(t) - x) + \delta(x - x_{w_1}(t))(-1)^{n_{w_1}(t)} + \delta(n_{w_1}(t))H(x - x_{w_1}(t)) \\ x_{w_1}(t) = (-1)^{n_{w_1}(t)}\left(ct - 2\left[\frac{n_{w_1}(t)+1}{2}\right]L_{tu}\right) \\ n_{w_1}(t) = \left[\frac{ct}{L_{tu}}\right] \end{cases} \quad (10)$$

(2) Tail-entry-induced PWS

$$\begin{cases} p_{s_{w_2}}(x,t) = sgn(x - x_{w_2}(t)) - \delta(x - x_{w_2}(t))(-1)^{n_{w_2}(t)} - \delta(n_{w_2}(t))H(x - x_{w_2}(t)) \\ x_{w_2}(t) = (-1)^{n_{w_2}(t)}\left(c(t - t_0) - 2\left[\frac{n_{w_2}(t)+1}{2}\right]L_{tu}\right) \\ n_{w_2}(t) = \left[\frac{c(t-t_0)}{L_{tu}}\right] \\ t_0 = \frac{L_{tr}}{v_{tr}} \end{cases} \quad (11)$$

(3) Nose-exit-induced PWS

$$\begin{cases} p_{s_{w_3}}(x,t) = sgn(x - x_{w_3}(t)) + \delta(x - x_{w_3}(t))(-,,,1)^{(t)}_{n_{w_3}} + \delta(n_{w_3}(t))H(x_{w_3}(t) - x) \\ x_{w_3}(t) = (-1)^{n_{w_3}(t)}\left(\left(2\left[\frac{n_{w_3}(t)}{2}\right] + 1\right)L_{tu} - c(t - t_1)\right) \\ n_{w_3}(t) = \left[\frac{c(t-t_1)}{L_{tu}}\right] \\ t_1 = \frac{L_{tu}}{v_{tr}} \end{cases} \quad (12)$$

(4) Tail-exit-induced PWS

$$\begin{cases} p_{s_{w_4}}(x,t) = sgn(x_{w_4}(t) - x) - \delta(x - x_{w_4}(t))(-1)^{n_{w_4}(t)} - \delta(n_{w_4}(t))H(x_{w_4}(t) - x) \\ x_{w_4}(t) = (-1)^{n_{w_4}(t)}\left(\left(2\left[\frac{n_{w_4}(t)}{2}\right] + 1\right)L_{tu} - c(t - t_0 - t_1)\right) \\ n_{w_4}(t) = \left[\frac{c(t-t_0-t_1)}{L_{tu}}\right] \end{cases} \quad (13)$$

In Equations (9) and (14), $x_{p_i}(t)$ describes the moving path of the PP induced by the train nose/tail, and the subscript i = 1, 2 is used to distinguish the PP induced by the train nose/tail. For the nose-induced PP, its influence starts from the moment when the train nose enters the tunnel (t = 0) to the moment when the train nose exits the tunnel ($t = L_{tu}/v_{tr}$). For the tail-induced PP, it generates from the moment when the train tail enters the tunnel ($t = L_{tr}/v_{tr}$) to the moment when the tail exits from the tunnel ($t = (L_{tu} + L_{tr})/v_{tr}$). $p_{s_{p_\mathrm{i}}}(x,t)$ describes the pressure state distribution in the tunnel influenced by PP, and the first term on the right describes the pressure state distribution $p_s(x)$ accurately, except for the case of

$x = x_p$, then the second term on the right supplements the condition of $x = x_p$, as mentioned in Section 3.2.2.

(5) PP induced by the train nose is represented by Equation (9).
(6) PP induced by the train tail

$$\begin{cases} p_{s_{p_2}}(x,t) = H\left(x_{p_2}(t) - x\right) + \delta\left(x - x_{p_2}(t)\right) \\ x_{p_2}(t) = v_{tr}t - L_{tr} \quad \left(\frac{L_{tr}}{v_{tr}} \le t \le \frac{L_{tu}+L_{tr}}{v_{tr}}\right) \end{cases} \tag{14}$$

As mentioned before, the principle of superposition applies to linear equations, such as Equations (9)–(14). Thus, for the point at x_0 m away from the entrance, its pressure state $p_s(x_0, t_k)$ at time t_k can be calculated as follows:

$$p_s(x_0, t_k) = \sum_{i=1}^{j} p_{s_{w_i}}(x_0, t_k) + \sum_{i=1}^{j} p_{s_{p_i}}(x_0, t_k) \tag{15}$$

where j represents the number of the influential PWSs and PP induced by train ends. In this paper, j is set as 4 for PWS and 2 for PP.

Then, the pressure of the measuring point is calculated as follows:

$$P(x_0, t_k) = p_s(x_0, t_k) f(\alpha) \tag{16}$$

where $f(\alpha)$ is determined using field measurements (such as train speed, blocking ratio, wave attenuation coefficient, etc.) [5,48] and research on pressure amplitude during train passage [24–26].

3.2.4. Definition of the Extreme Pressure and Pressure Regions

According to the time sequence, Equations (9) and (12), Equations (13) and (14) do not coincide in time. Thus, the maximum and minimum values of p_s are ± 4. The condition where p_s could reach $\pm$ 4 is called the worst condition.

In the post-train stage, p_s = 4 represents that during a short time, the pressure in the tunnel rises continuously due to the influence of the successive compression waves from four PWSs, as shown in labels 17–20 in Figure 1. p_s = -4 indicates that in a short time, the pressure continuously decreases under the influence of the successive expansion waves from the four PWSs, as shown in labels 13–16 in Figure 1. In the worst condition, the region where p_s could reach 4 is called the positive pressure region, and those with p_s = -4 are called the negative pressure regions, where the positive and negative pressure amplitudes are greater than the other region of the tunnel.

The intersection of the positive and negative pressure regions is the peak pressure region, where the pressure fluctuates greatly. MPP is the point where the pressure rises for the longest time in the positive pressure region. MNP is the point with the longest pressure drop time in the negative pressure region. MPP and MNP are also called extreme pressure. The MPPR is the region with MPP and MNP as the endpoints, indicating where the maximum peak-to-peak pressure (the largest difference between the positive and negative pressure peaks) would appear after train passage. It is usually the place with serious fatigue damage due to the largest alternating load.

Owing to the attenuation during wave propagation, only the superposition of the influential pressure waves (with less attenuation) is considered in this study. European standards EN 14067-5 [49] indicate that in the post-train stage, the pressure fluctuation is still significant for a period ($\le$10 L_{tu}/c). Thus, in this study, for the entry-induced PWS, $n_w \le 10$, for the exit-induced PWS, $n_w \le 4$.

3.2.5. Prediction of Extreme Pressure in the Tunnel and Calculation Program

The proposed SDPS model applies to cases with different pressure states; here, we mainly focus on the distribution of extreme pressures under the worst conditions (where the superimposed pressure state can reach +4 or −4). As shown in Figure 6, first, four parameters (L_{tu}, L_{tr}, v_{tr} and c) are used to describe the investigated case and qualitatively judge whether the case is the worst condition. Second, if it is the worst condition, the pressure region, MPP, MNP, and the MPPR, which are caused by the superposition of the PWSs or PPs, are identified by calculating Equations (9)–(15). Finally, the occurrence time and location of the extreme pressure are the output.

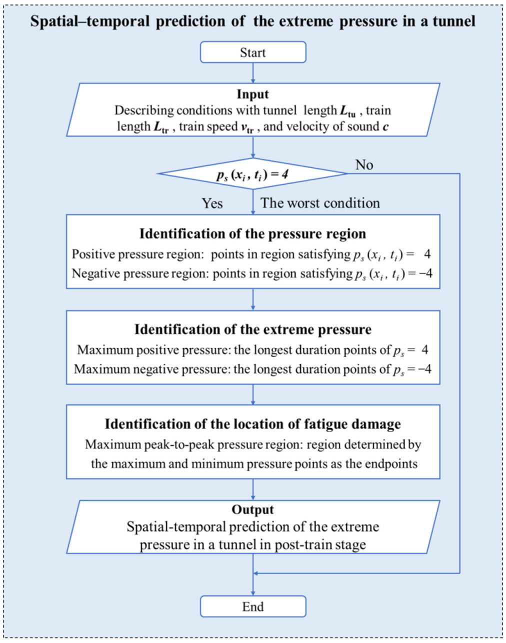

Figure 6. Flowchart of spatial–temporal prediction of the extreme pressure in a tunnel.

Based on the previous equations, a fast and accurate calculation program was developed using Python. The code of the calculation program is provided in the Supplementary Materials. The program could assist users in obtaining the calculated results within several seconds, which is much faster than the traditional method [23,27–29]. It is suitable for various situations, such as design, operation, and maintenance. It also has no special requirements for computer hardware. A common personal laptop can run this program. In addition, its accuracy has been verified using field measurements, as described in Section 4.1.

3.3. Dimensional Analysis

The dimensional analysis provides insight into the spatial–temporal prediction of extreme pressure in a tunnel, identifies nondimensional parameters, and obtains general results. The appearance of MPP and MNP is caused by the superposition of PWSs. As the time difference between entry-induced PWS and exit-induced PWS is L_{tu}/v_{tr} (corresponds to the train passing time in the tunnel), and between nose-induced PWS and tail-induced, PWS is L_{tr}/v_{tr} (corresponds to the passing time of train body). The characteristic time of pressure wave propagation in the tunnel is L_{tu}/c. The location and time of the extreme pressure in the tunnel are x and t, respectively. Thus, the issue concerning their position and time of appearance involves six variables, which are L_{tu}, L_{tr}, v_{tr}, c, x, and t, but only two fundamental dimensions, length L and time T. According to Buckingham's π theorem [50], $6 - 2 = 4$ dimensionless products are determined, as shown in Equations (17)–(20).

$$M = \frac{v_{tr}}{c} = \frac{\frac{L_{tu}}{c}}{\frac{L_{tu}}{v_{tr}}} \tag{17}$$

$$\varepsilon = \frac{L_{tr}}{L_{tu}} \tag{18}$$

$$x^* = \frac{x}{L_{tu}} \tag{19}$$

$$t^* = \frac{t}{\frac{L_{tu}}{c}} \tag{20}$$

The train/wave velocity ratio M is the ratio of the train speed to the local velocity of sound and represents the relative magnitude of the pressure wave propagation time L_{tu}/c and the characteristic time of the train passing through the tunnel L_{tu}/v_{tr}. The train/tunnel length ratio ε is the ratio of the train length to the tunnel length. The dimensionless position of the extreme pressure x^* indicates the relative position of extreme pressure in the tunnel. The dimensionless time of the extreme pressure t^* is the ratio of the appearance time t to the characteristic time of pressure wave propagation L_{tu}/c.

Therefore, the relationship between the six variables can be given by the following:

$$x^* = F(M, \varepsilon) \tag{21}$$

$$t^* = F(M, \varepsilon) \tag{22}$$

where the symbol F only represents a relationship, not a specific function. Equations (21) and (22) show that the dimensionless location and time of extreme pressures in a tunnel are related to M and ε, and M and ε could be used to describe the different operating conditions. If the dimensionless quantities of M and ε are used to describe the conditions in Figure 6, then the dimensionless results would be obtained accordingly.

In addition, the frequency of the pressure fluctuation in the post-train stage can be calculated as Equation (23), which is related to fatigue damage.

$$f = \frac{1}{T} = \frac{c}{2L_{tu}} \tag{23}$$

4. Results and Discussion

4.1. Validation of the Proposed SDPS Model

A 201.4-m-long CRH2C passes through two tunnels at a speed of 300 km/h. The tunnel lengths are 1005 m and 2812 m, and the local velocity of sound is 336 m/s (1 standard atmospheric pressure, 283.15 K) [14]. Pressure-measuring points are deployed along the tunnel in the longitudinal direction in the field measurements, the measuring point intervals in the middle section of the 1005-m-long and 2812-m-long tunnels were 100 m and 200 m, respectively. Relative error (RE) is introduced to quantify the differences between the predicted and measured results [51]:

$$RE = \frac{|x_{pre} - x_{mea}|}{L_{tu}} \times 100\% \tag{24}$$

where x_{pre} is the predicted locations of the extreme pressure, and x_{mea} is the measured results.

As shown in Figure 7, in the 2812-m-long tunnel, the measured MPP and MNP both appear at 1400 m from the entrance, and the predicted MPP and MNP appeared at 1450.99 m and 1361.01 m, respectively. The REs were 1.81% and 1.39%, respectively.

As for the 1005-m-long tunnel, the measured MPP appeared at 500 m from the entrance at 15.70 s, and the predicted MPP appeared at 518.58 m at 15.49 s. The measured MNP appeared at 500 m at 18.45 s, and the predicted MNP appeared at 486.42 m at 18.92 s. The REs of the spatial distribution of MPP and MNP were 1.85% and 1.35%, respectively. The difference between the measured and predicted occurrence times is less than 0.5 s, and it is mainly from the position difference between the measured point and the predicted point of the SDPS model. The difference would be further reduced if the measured data at the predicted location (518.58 m and 486.42 m) were available. In general, the predicted results were in good agreement with the measured results and proved the validity of the SDPS model.

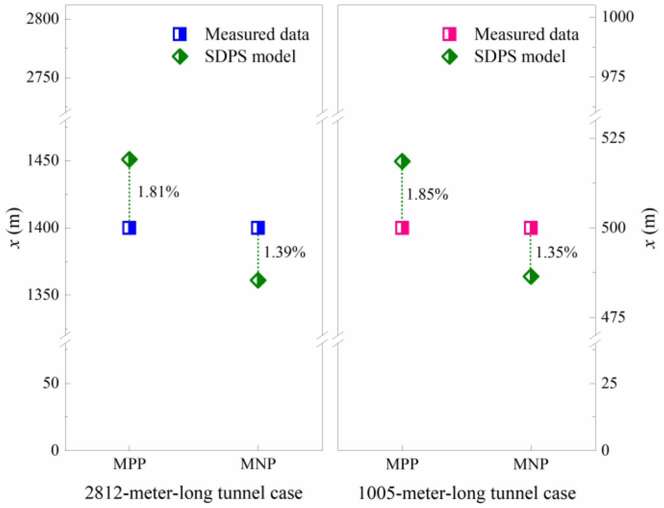

Figure 7. Comparison between the proposed SDPS model and field tests in two tunnels (MPP: maximum positive pressure, MNP: maximum negative pressure).

4.2. Spatial Distribution of the Extreme Pressure

Based on the SDPS model, the distribution of the extreme pressure and typical pressure regions under different cases (described by M and ε) were analyzed. Since the flow issue with a high Mach number would involve shock waves, this paper only investigated the pressure wave propagation with $M \leq 0.8$. As the train lengths in operation in China are approximately 200 m and 400 m, the three-dimensional effect should be considered for pressure fluctuations in tunnels within 50 m of the tunnel portals [52,53]. Therefore, ε is no more than 0.8 in the SDPS model.

Based on the dimensionless analysis, the dimensionless location and the time of the appearance of extreme pressure are associated with M and ε. Figure 8a,b depict the dimensionless spatial distribution of the MPP and MNP with M and ε as the abscissa, respectively (ε = 0.05, 0.1, 0.15, ... , 0.8 and M = 0.05, 0.1, 0.15, ... , 0.8). x^* = 0 corresponds to the tunnel entry, and x^* = 1 corresponds to the tunnel exit. The results show that the MPP and MNP are distributed in the region $x^* \in [0.33,0.71]$, and 99.2% of them are concentrated in the region $x^* \in [0.33,0.67]$.

Figure 9 shows the change in the location of the MPP and MNP with variations in M and ε ($M \leq 0.8$, $\varepsilon \leq 0.8$). The locations of the MPP and MNP are indicated by the dark and light one of the same colors, respectively. As shown in Figure 9, most of the MPPs and MNPs are symmetrical about the midpoint of the tunnel axis and appear alternately around it. This is because the MPP and MNP are mostly determined by the superposition of four PWSs. While in several cases, the determination of the MNPs needs to consider the influence of the PPs caused by the train tail. It results in the asymmetry in the location of the MPP and MNP, as shown in Figure 9a. For example, when M = 0.15 and ε = 0.2, the MPP appears at the midpoint of the tunnel axis x^* = 0.5 while the MNP appears at the position of x^* = 0.67, showing asymmetry.

In addition, in the post-train stage, the MPP is found to be determined by the superposition of PWSs, and MNP is related to the PWS and PP, which are similar to that during train passage [18,19].

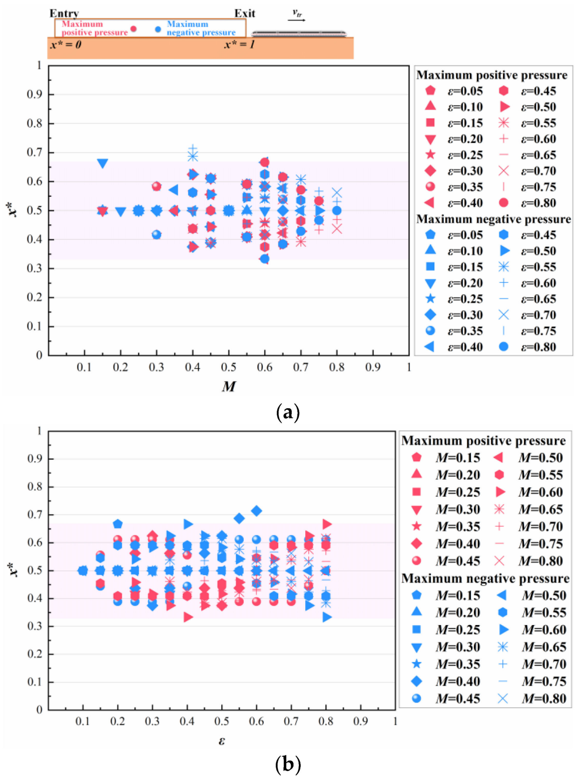

Figure 8. Distribution of the normalized location of the extreme pressure under different conditions ($M \leq 0.8$, $\varepsilon \leq 0.8$): (**a**) from the point of the train/wave velocity ratio M; and (**b**) from the point of the train/tunnel length ratio ε.

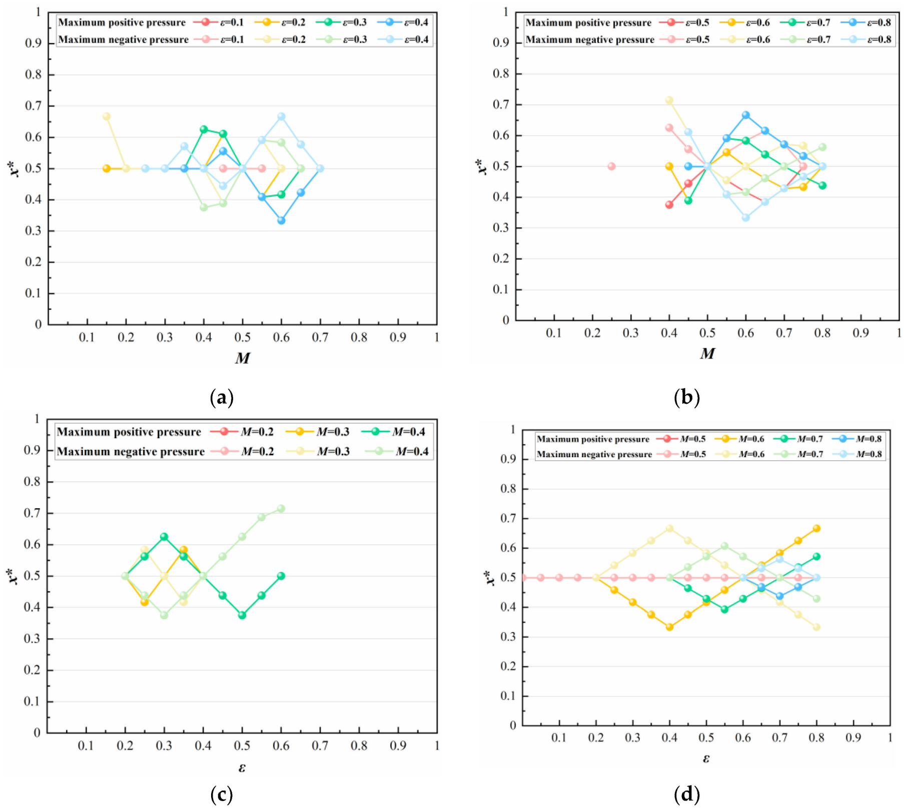

Figure 9. Change in the location of the maximum positive and negative pressures with different train/wave velocity ratios M and train/tunnel length ratios ε: (**a**) ε = 0.1–0.4, $M \leq 0.8$; (**b**) ε = 0.5–0.8, $M \leq 0.8$; (**c**) M = 0.1–0.4, $\varepsilon \leq 0.8$; and (**d**) M = 0.5–0.8, $\varepsilon \leq 0.8$.

4.3. Fatigue Damage: Distribution of the Maximum Peak-to-Peak Pressure Region

As shown in Figure 10a–d, when $\varepsilon \in [0.1, 0.4]$ (passing through a tunnel longer than 500 m), the MPPR is located in the region of [0.33,0.67]. As seen from Figure 10e–h, when $\varepsilon \in [0.4,0.8]$, the MPPR is located in the region of [0.33,0.71]. When $M \in [0.1,0.4]$ (corresponding to $v_{tr} < 500$ km/h), the MPPR is located in the region of [0.38,0.71]; when $M \in [0.4,0.8]$, the MPPR is located in the region of [0.33,0.67]. Thus, MPPR is mainly located in the region $x^* \in [0.33,0.67]$, indicating the most probable location of accidents caused by fatigue failure. As there are some pressure-bearing facilities in the tunnel, such as fire doors, control boxes, and signal lights, it is suggested to reinforce the tunnel lining and facilities and avoid placing auxiliary facilities in the MPPR.

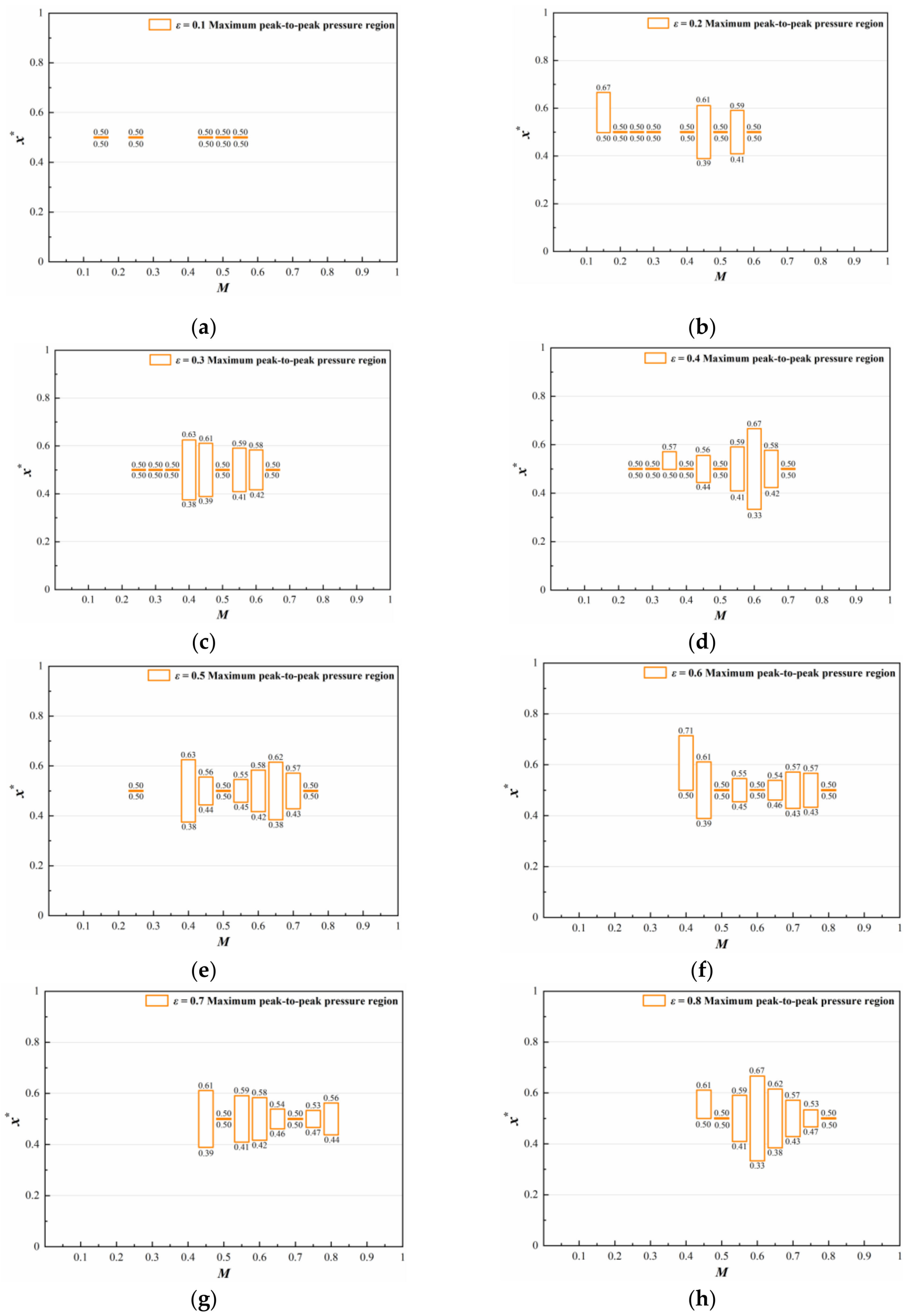

Figure 10. Distribution of the maximum peak-to-peak pressure region under different train/wave velocity ratios M and train/tunnel length ratios ε ($M \leq 0.8$, $\varepsilon \leq 0.8$): (**a**) $\varepsilon = 0.1$; (**b**) $\varepsilon = 0.2$; (**c**) $\varepsilon = 0.3$; (**d**) $\varepsilon = 0.4$; (**e**) $\varepsilon = 0.5$; (**f**) $\varepsilon = 0.6$; (**g**) $\varepsilon = 0.7$; and (**h**) $\varepsilon = 0.8$.

In addition, Figure 10 shows that when M = 0.5 with ε = 0.1–0.8 (the corresponding train speed is approximately 600 km/h), and when M = 0.25 with ε = 0.1–0.5 (the corresponding speed is approximately 300 km/h), both the MPP and MNP appear at the midpoint of the tunnel axis in the worst conditions. This result indicates that under the conditions calculated above, no matter how long the tunnel is, the midpoint of the tunnel axis is the worst pressure fluctuation point in the tunnel associated with failure damage.

5. Conclusions

This paper focused on the spatial–temporal distribution of extreme pressures in high-speed railway tunnels and its long-term effects on the safety of the transportation system in the post-train stage. Based on the evolution and superpositions of pressure waves, a one-dimensional model referred to as the spatial–temporal distribution of the pressure state (SDPS) model is developed, and equations are first proposed to describe the pressure state variation with time and space in the tunnel. Based on the SDPS model, a spatial–temporal prediction method for the extreme pressure in a tunnel and a calculation program are developed, which can greatly reduce the calculation cost and time in the tunnel design stage. Finally, the dimensionless spatial distribution of the extreme parameters (MPP, MNP, and MPPR) in the tunnel under different working conditions is analyzed using dimensionless operation parameters (train/wave velocity ratio M and train/tunnel length ratio ε). The main conclusions are summarized as follows:

(1) The pressure wave in the tunnel follows the principle of wave superposition, which can be calculated quickly with the SDPS model proposed in this study. The proposed model was verified by the field measurements, and the relative errors of the predicted and measured MPP and MNP are between 1.35% and 1.85%.
(2) In the post-train stage, the MPP is determined by the superposition of PWS, and MNP is related to PWS and PP. When the MPP and MNP are only determined by the superposition of the PWSs, they are symmetrical about the midpoint of the tunnel axis and appear alternately around it. Otherwise, it would result in asymmetry in the location of the MPP and MNP.
(3) When $M \in [0.1, 0.8]$ and $\varepsilon \in [0.1, 0.8]$, the dimensionless positions of the MPP, MNP, and MPPR are concentrated in the middle region of the tunnel ($x/L_{tu} \in [0.33, 0.67]$); meaning that the tunnel lining and facilities should be strengthened in the MPPR of the built tunnel to prevent fatigue failure. In the future, avoid placing pressure-bearing tunnel facilities (such as fire doors, control boxes, signal lights, etc.) in the MPPR to extend the life span of tunnel facilities.

It should be noted that due to the three-dimensional effect, the SDPS model may need to be modified within 50 m of the tunnel entrance, which will be discussed in the future.

Supplementary Materials: The following supporting information can be downloaded at: https://www.mdpi.com/article/10.3390/app13031350/s1.

Author Contributions: Conceptualization, W.L., A.L., H.C. and L.C.; methodology, W.L., A.L., H.C. and L.C.; software, W.L.; validation, W.L.; formal analysis, W.L.; investigation, W.L.; resources, A.L. and H.C.; funding acquisition, L.C.; supervision, A.L., H.C. and L.C.; writing—original draft, W.L.; writing—review & editing, A.L. and H.C. All authors have read and agreed to the published version of the manuscript.

Funding: The author Li Chen was funded by the Natural Science Foundation of Shaanxi Province, and the grant number is 2020JM-479.

Acknowledgments: Thanks are extended to Bo Lei, Honglin Wang, Lunfei Che, Jialiang Wang for their constructive suggestions, Pengpeng Shi for the inspire of the function related with n_w, and Zhiyuan Liu, Yuqing Bai for assistance in program development.

Conflicts of Interest: The authors declare no conflict of interest.

Nomenclature/Abbreviations

c	the velocity of sound (m/s)
L_{tr}	train length (m)
L_{tu}	tunnel length (m)
M	train/wave velocity ratio
n_w	the reflected times of the wave at the tunnel port at t time
p	pressure (Pa)
p_s	pressure state
p_{swi}	pressure fluctuation state of the measuring point influenced by pressure wave (i = 1, 2, 3, . . .)
p_{spi}	pressure fluctuation state of the measuring point influenced by pressure pulse (i = 1, 2, 3, . . .)
t	time (s)
v_{tr}	train speed (m/s)
x_{wi}	position of the pressure wave in a tunnel (i = 1, 2, 3, . . .)
x_{pi}	position of the pressure pulse in a tunnel (i = 1, 2)
x_{pre}	predicted location of the extreme pressure
x_{mea}	measured location of the extreme pressure
ε	train/tunnel length ratio
superscript*	dimensionless variables
SDPS	spatial–temporal distribution of the pressure state
MPP	maximum positive pressure
MPPR	maximum peak-to-peak pressure region
MNP	maximum negative pressure
PP	pressure pulse
PWS	pressure wave system
RE	relative error

References

1. Du, J.; Fang, Q.; Wang, G.; Zhang, D.; Chen, T. Fatigue damage and residual life of secondary lining of high-speed railway tunnel under aerodynamic pressure wave. *Tunn. Undergr. Space Technol.* **2021**, *111*, 103851. [CrossRef]
2. Li, C.; Liu, M.; Chang, R.; Wang, X.; Liu, W.; Zhang, H. Air pressure and comfort study of the high-speed train passing through the subway station. *Sustain. Cities Soc.* **2022**, *81*, 103881. [CrossRef]
3. Niu, J.Q.; Zhou, D.; Liang, X.F.; Liu, S.; Liu, T.H. Numerical simulation of the Reynolds number effect on the aerodynamic pressure in tunnels. *J. Wind Eng. Ind. Aerod.* **2018**, *173*, 187–198. [CrossRef]
4. Li, F.; Luo, J.; Wang, L.; Guo, D.; Gao, L. Analysis of aerodynamic effects and load spectrum characteristics in high-speed railway tunnels. *J. Wind Eng. Ind. Aerod.* **2021**, *216*, 104729. [CrossRef]
5. Liu, F.; Zhou, W.; Niu, J.Q.; Zhang, J. Impact of increased linings on pressure transients induced by a train passing through a tunnel. *Sustain. Cities Soc.* **2019**, *45*, 314–323. [CrossRef]
6. Wang, T.; Han, X.; Zhang, L.; Qian, B.; Sun, Z.; Liu, H. Effect of non-circular tunnel linings on pressure transients induced by high-speed train passes through a tunnel based on moving model test. *J. Wind Eng. Ind. Aerod.* **2021**, *214*, 104649. [CrossRef]
7. Heine, D.; Ehrenfried, K.; Kühnelt, H.; Lachinger, S.; Rudolph, M.; Vorwagner, A.; Saliger, F. Influence of the shape and size of cavities on pressure waves inside high-speed railway tunnels. *J. Wind Eng. Ind. Aerod.* **2019**, *189*, 258–265. [CrossRef]
8. Liu, T.H.; Jiang, Z.H.; Chen, X.D.; Zhang, J.; Liang, X.F. Wave effects in a realistic tunnel induced by the passage of high-speed trains. *Tunn. Undergr. Space Technol.* **2019**, *86*, 224–235. [CrossRef]
9. Peng, Y.; Wu, Z.; Fan, C.; Zhou, J.; Yi, S.; Peng, Y.; Gao, K. Assessment of passenger long-term vibration discomfort: A field study in high-speed train environments. *Ergonomics.* **2021**, *65*, 659–671. [CrossRef]
10. Asakura, T.; Kojima, Y. Tunnel maintenance in Japan. *Tunn. Undergr. Space Technol.* **2003**, *18*, 161–169. [CrossRef]
11. Shi, C.-H.; Wang, A.; Sun, X.-H.; Yang, W.-C. Aerodynamic Behavior and Impact on Driving Safety of Spalling Blocks Comprising High-Speed-Railway Tunnel Lining. *Appl. Sci.* **2022**, *12*, 2593. [CrossRef]
12. Yang, W.; Deng, E.; Shi, C.; Liu, N.; Fei, R.; Yue, H. Lining Fatigue Test and Influence Zoning of Tridimensional Cross-Tunnel under High-Speed Train Loads. *Appl. Sci.* **2020**, *10*, 5694. [CrossRef]
13. Ricco, P.; Baron, A.; Molteni, P. Nature of pressure waves induced by a highspeed train travelling through a tunnel. *J. Wind Eng. Ind. Aerod.* **2007**, *95*, 781–808. [CrossRef]
14. Liu, F.; Yao, S.; Zhang, J.; Wang, Y.Q. Field measurements of aerodynamic pressures in high-speed railway tunnels. *Tunn. Undergr. Space Technol.* **2018**, *72*, 97–106. [CrossRef]

15. William-Louis, M.P.; Gregoire, R. 1-D calculations of pressure fluctuations outside and inside a pressure sealed high-speed trainset travelling through tunnels. In *TRANSAERO—A European Initiative on Transient Aerodynamics for Railway System Optimisation*; Springer: Berlin/Heidelberg, Germany, 2002; pp. 342–357. [CrossRef]
16. Li, F.; Luo, J.; Wang, D.; Wang, L. Aerodynamic Characteristics When Trains Pass Each Other in High-Speed Railway Shield Tunnel. *Appl. Sci.* **2022**, *12*, 6244. [CrossRef]
17. He, D.H.; Chen, H.C.; Zhang, Y.; Huang, T.Z.; Huang, C.R. Theoretical analysis and experimental investigation of the occurrence location of the largest negative pressure. *Rail. Loco. Car.* **2011**, *31*, 3. [CrossRef]
18. Ko, Y.Y.; Chen, C.H.; Hoe, T.; Wang, S.T. Field measurements of aerodynamic pressures in tunnels induced by high speed trains. *J. Wind Eng. Ind. Aerod.* **2012**, *100*, 19–29. [CrossRef]
19. Li, R.X.; Yuan, L. Pressure waves in tunnels when high-speed train passing through. *J. Mech. Eng.* **2014**, *50*, 115–121. [CrossRef]
20. Somaschini, C.; Argentini, T.; Brambilla, E.; Rocchi, D.; Schito, P.; Tomasini, G. Full-Scale Experimental Investigation of the Interaction between Trains and Tunnels. *Appl. Sci.* **2020**, *10*, 7189. [CrossRef]
21. Johnson, T.; Dalley, S. 1/25 scale moving model tests for the TRANSAERO Project. In *TRANSAERO—A European Initiative on Transient Aerodynamics for Railway System Optimisation*; Springer: Berlin/Heidelberg, Germany, 2002; pp. 123–135. [CrossRef]
22. Zhang, L.; Yang, M.Z.; Niu, J.Q.; Liang, X.F.; Zhang, J. Moving model tests on transient pressure and micro-pressure wave distribution induced by train passing through tunnel. *J. Wind Eng. Ind. Aerod.* **2019**, *191*, 6. [CrossRef]
23. Guo, Z.; Liu, T.; Hemida, H.; Chen, Z.; Liu, H. Numerical simulation of the aerodynamic characteristics of double unit train. *Eng. Appl. Comp. Fluid.* **2020**, *14*, 910–922. [CrossRef]
24. Hara, T. Aerodynamic force acting on a high-speed train at tunnel entrance. *Bull. JSME* **1961**, *4*, 547–553. [CrossRef]
25. Howe, M.S.; Iida, M.; Fukuda, T.; Maeda, T. Theoretical and experimental investigation of the compression wave generated by a train entering a tunnel with a flared portal. *J. Fluid. Mech.* **2000**, *425*, 111–132. [CrossRef]
26. Sockel, H. Aerodynamic effects caused by a train entering a tunnel. In *PAMM: Proceedings in Applied Mathematics and Mechanics*; WILEY-VCH Verlag Berlin GmbH: Berlin, Germany, 2002; pp. 268–269.
27. Li, W.H.; Liu, T.H.; Martinez-Vazquez, P.; Chen, Z.W.; Guo, Z.J.; Li, M.; Xia, Y.T.; Liu, H.K. Aerodynamic effects of a high-speed train travelling through adjoining & separated tunnels. *Tunn. Undergr. Space Technol.* **2021**, *113*, 103973. [CrossRef]
28. Liang, X.F.; Chen, G.; Li, X.B.; Zhou, D. Numerical simulation of pressure transients caused by high-speed train passage through a railway station. *Build. Environ.* **2020**, *184*, 107228. [CrossRef]
29. Niu, J.Q.; Zhou, D.; Liu, F.; Yuan, Y. Effect of train length on fluctuating aerodynamic pressure wave in tunnels and method for determining the amplitude of pressure wave on trains. *Tunn. Undergr. Space Technol.* **2018**, *80*, 277–289. [CrossRef]
30. Mashimo, S.; Nakatsu, E.; Aoki, T.; Matsuo, K. Entry Compression Wave Generated by a High-Speed Train Entering a Tunnel. *Trans. Jpn. Soc. Mech. Eng. Part B* **1995**, *61*, 3720–3727. [CrossRef]
31. Matsuo, K.; Aoki, T.; Kashimura, H.; Nonaka, Y. Emission of a Propagating Compression Wave from an Open End of a Tube (1st report, analytical Study). *Trans. Jpn. Soc. Mech. Eng. Part B* **1992**, *58*, 331–337. [CrossRef]
32. Liu, T.H.; Chen, Z.W.; Chen, X.D.; Xie, T.Z.; Zhang, J. Transient loads and their influence on the dynamic responses of trains in a tunnel. *Tunn. Undergr. Space Technol.* **2017**, *66*, 121–133. [CrossRef]
33. Baron, A.; Mossi, M.; Sibilla, S. The alleviation of the aerodynamic drag and wave effects of high-speed trains in very long tunnels. *J. Wind Eng. Ind. Aerod.* **2001**, *89*, 365–401. [CrossRef]
34. Woods, W.A.; Pope, C.W. A generalised flow prediction method for the unsteady flow generated by a train in a single-track tunnel. *J. Wind Eng. Ind. Aerod.* **1981**, *7*, 331–360. [CrossRef]
35. Tabarra, M.; Sturt, R.; Arup, U.K. High Speed Rail Tunnel Aerodynamics: Transient pressure and loadings on fixed tunnel equipment. In Proceedings of the 7th UIC World Congress on High Speed Rail, Beijing, China, 7–9 December 2010.
36. Liu, F.; Yao, S.; Liu, T.H.; Zhang, J. Analysis on aerodynamic pressure of tunnel wall of high-speed railways by full-scale train test. *J. Zhejiang Univ.* **2016**, *50*, 2018–2024. [CrossRef]
37. Aguilar, L.A.; Robledo-Sanchez, C.; Carrasco, M.A.; Otero, M.M. The principle of superposition for waves: The amplitude and phase modulation phenomena. *Appl. Math. Inform. Sci.* **2012**, *6*, 307–315.
38. Reilly, T.E.; Franke, O.L.; Bennett, G.D. The principle of superposition and its application in ground-water hydraulics. In *U.S. Geological Survey, Techniques of Water-Resources Investigations*; Book 3; Chapter B6; USGS: Reston, VA, USA, 1987.
39. Du, J.; Fang, Q.; Wang, J.; Wang, G. Influences of High-Speed Train Speed on Tunnel Aerodynamic Pressures. *Appl. Sci.* **2022**, *12*, 303. [CrossRef]
40. Zhou, C.H. *Numerical Study on Pressure Waves Produced by Trains in Complex Tunnel*; Lanzhou Jiaotong University: Lanzhou, China, 2016.
41. Li, W.H.; Liu, T.H.; Chen, Z.W.; Guo, Z.J.; Huo, X.S. Comparative study on the unsteady slipstream induced by a single train and two trains passing each other in a tunnel. *J. Wind Eng. Ind. Aerod.* **2020**, *198*, 104095. [CrossRef]
42. Raghunathan, R.S.; Kim, H.D.; Setoguchi, T. Aerodynamics of high-speed railway train. *Prog. Aerosp. Sci.* **2002**, *38*, 469–514. [CrossRef]
43. Li, W.H.; Liu, T.H.; Huo, X.S.; Chen, Z.W.; Guo, Z.J.; Li, L. Influence of the enlarged portal length on pressure waves in railway tunnels with cross-section expansion. *J. Wind Eng. Ind. Aerod.* **2019**, *190*, 10–22. [CrossRef]
44. Sockel, H. Formulae for the Calculation of Pressure Effects in Railway Tunnels. In Proceedings of the 11th International Symposium on Aerodynamics and Ventilation of Vehicle Tunnels, Luzern, Switzerland, 7–9 July 2003; pp. 581–595.

45. Wang, T.T.; Wu, F.; Yang, M.Z.; Ji, P.; Qian, B.S. Reduction of pressure transients of high-speed train passing through a tunnel by cross-section increase. *J. Wind Eng. Ind. Aerod.* **2018**, *183*, 235–242. [CrossRef]
46. Zhou, D.; Tian, H.Q.; Zhang, J.; Yang, M.Z. Pressure transients induced by a high-speed train passing through a station. *J. Wind Eng. Ind. Aerod.* **2014**, *135*, 6. [CrossRef]
47. Liang, X.F.; Li, X.B.; Chen, G.; Sun, B.; Wang, Z.; Xiong, X.H.; Yin, J.; Tang, M.Z.; Li, X.L.; Krajnović, S. On the aerodynamic loads when a high speed train passes under an overhead bridge. *J. Wind Eng. Ind. Aerod.* **2020**, *202*, 104208. [CrossRef]
48. Vardy, A.E.; Brown, J. An overview of wave propagation in tunnels. In *TRANSAERO—A European Initiative on Transient Aerodynamics for Railway System Optimisation*; Springer: Berlin/Heidelberg, Germany, 2002; pp. 249–266. [CrossRef]
49. *EN14067-5*; Railway Applications-Aerodynamics-Part 5: Requirements and Test Procedures for Aerodynamics in Tunnels. European Standard: Brussels, Belgium, 2018.
50. Buckingham, E. On physically similar systems; illustrations of the use of dimensional Equations. *Phys. Rev.* **1914**, *4*, 345. [CrossRef]
51. Wei, Y.; Zhou, H.; Zhang, T.T.; Wang, S. Inverse identification of multiple temporal sources releasing the same tracer gaseous pollutant. *Build Environ.* **2017**, *118*, 184–195. [CrossRef]
52. Auvity, B.; Bellenoue, M.; Kageyama, T. Experimental study of the unsteady aerodynamic field outside a tunnel during a train entry. *Exp. Fluids.* **2001**, *30*, 221–228. [CrossRef]
53. Bellenoue, M.; Moriniere, V.; Kageyama, T. Experimental 3-D simulation of the compression wave, due to train–tunnel entry. *J. Fluid. Struct.* **2002**, *16*, 581–595. [CrossRef]